

## Evaluation of the Corrosion Inhibition Performance of Silane Coatings Filled with Cerium Salt-Activated Nanoparticles on Hot-Dip Galvanized Steel Substrates

Roohangiz Zandi Zand<sup>1</sup>, Kim Verbeken<sup>2</sup>, Annemie Adriaens<sup>1,\*</sup>

<sup>1</sup>Department of Analytical Chemistry, Ghent University, Krijgslaan 281-S12, B-9000, Ghent, Belgium

<sup>2</sup>Department of Materials Science and Engineering, Ghent University, Technologiepark 903, B-9052 Zwijnaarde (Ghent), Belgium

\*E-mail: [annemie.adriaens@ugent.be](mailto:annemie.adriaens@ugent.be)

Received: 22 January 2013 / Accepted: 12 March 2013 / Published: 1 April 2013

---

The present work investigates the morphological and electrochemical behavior of hot-dip galvanized (HDG) steel substrates that were pre-treated with 3-glycidoxypropyltrimethoxysilane (GPTMS) and bisphenol A (BPA) modified with cerium ion-activated CeO<sub>2</sub> nanoparticles. The morphology of the coatings before and after the corrosion test was examined using atomic force microscopy (AFM) and scanning electron microscopy (SEM). The results indicated the formation of a comparatively smooth, nanostructured surface, with a small heterogeneity in the coating thickness. Microscopic observations also confirmed that the integral surface morphology of the silane coating filled with activated CeO<sub>2</sub> nanoparticles was maintained after short-term corrosion tests (144 h). The corrosion behavior of the sol-gel coatings was investigated using natural salt spray tests, electrochemical impedance spectroscopy (EIS), and potentiodynamic polarization tests. The results showed that the presence of the nanoparticles reinforced the barrier properties of the silane films, and a synergy seemed to be created between the activated nanoparticles and the cerium ions, reducing the corrosion activity.

---

**Keywords:** CeO<sub>2</sub> nanoparticles; Cerium nitrate; Galvanized steel; Corrosion inhibition; Silane coating.

### 1. INTRODUCTION

Zinc coatings are predominantly used for an improved aqueous corrosion resistance of steel by two mechanisms, namely barrier and galvanic protection. On the one hand, the zinc coating serves as a barrier between the steel substrate and the corrosive environment. Consequently zinc will be attacked before steel. On the other hand, since zinc is less noble, i.e. more anodic than iron at ambient conditions, it will also offer galvanic protection as zinc will sacrificially corrode to protect the steel substrate, even if steel is exposed at cut edges or at scratches. Typical processing methods used to

apply Zn-based coatings include hot-dip galvanizing (HDG), thermal spraying and electro deposition. HDG is the immersion of a steel compound in a molten bath of zinc or a zinc-alloy. Both batch and continuous processing methods are industrially available [1]. An extensive overview of the metallurgy of zinc coated steels can be found in the review of Marder [2].

The corrosion resistance of HDG steel can be improved by the application of coatings [2]. One approach to improve corrosion resistance of HDG steel is based on hybrid organic–inorganic coatings [3-4]. This approach combines the advantages of the inorganic and organic components. The organic constituent provides flexibility, reduces defectiveness, and improves the compatibility with the polymer coatings, while the inorganic part is responsible for the superior adhesion to the metal surface and the high ductility. Moreover, these coatings can be applied at relatively low temperatures.

The anticorrosive properties of hybrid organic–inorganic coatings can be improved by the incorporation of nanoparticles in the coating [5-18]. The nanoparticles can be synthesized in the films, as demonstrated for sol–gel coatings [9-11], or they can be added to the pre-treatment solutions [13]. The corrosion resistance of Mg alloys, pre-treated with sol–gel coatings containing  $ZrO_2$  and  $CeO_2$  nanoparticles, has been investigated previously, and it was reported that the  $CeO_2$  component provided enhanced corrosion protection, while  $ZrO_2$  imparted corrosion resistance and wear resistance [19].

Van Ooij and co-workers [14] reported that bis-sulfur silane films could be thickened and strengthened by loading them with silica particles. However, when the bis-sulfur silane film was heavily loaded with silica, it tended to form a porous film, which promoted electrolyte intrusion and premature film delamination. The addition of  $SiO_2$  nanoparticles to silane films electrodeposited on aluminum also revealed beneficial effects, and a “critical content” of nanoparticles was proposed [15]. The results obtained in these studies focused mainly on the role of the nanoparticles in the barrier properties of the film, and little attention was given at the role of the nanoparticles in the electrochemical processes involved in the corrosion processes of metallic substrates [9].

Ceria nanoparticles are versatile materials that have found applications in many different fields, including catalysis [20], ceramics [21], fuel cells [21] sensors [22-23], biomaterials [24], cosmetics [8], and coatings [25-26]. With respect to coatings, ceria nanoparticles have shown to improve wear and corrosion resistance in acidic media [26]. NiAl intermetallic coatings containing  $CeO_2$ , in comparison with the coating without  $CeO_2$ , exhibited higher hardness, an improved elastic modulus, fewer defects, and decreased porosity [27].  $Ce_2O_3$ – $CeO_2$  layers showed a pronounced stabilizing effect on the passive state of steel and its corrosion resistance in a sulfuric acid medium, which allows these coated steels to be used as construction materials for reactors neutralizing sulfuric acid-containing emissions [28]. It has also been reported that nano- $CeO_2$  and nano- $SiO_2$  particles increased the thermal stability of Ni–W–P alloy coatings at high temperatures, and improved their micro-hardness [29].

Previous work has reported the protective nature of silane coatings modified with  $CeO_2$  nanoparticles and cerium nitrate [30-32]. The results demonstrated that ceria nanoparticles were very effective fillers; they led to improved barrier properties in the silane coatings, and improved the corrosion inhibition. It was established that the positive impact on both the barrier properties and the corrosion inhibition was significantly improved by modifying the silane solution with cerium nitrate. The presence of cerium nitrate reinforced the barrier properties of the silane films, reducing the corrosion activity and improved self-healing the corroded areas.

The present work reports and discusses the protective behavior of silane films loaded with CeO<sub>2</sub> nanoparticles. The nanoparticles were activated with cerium ions to improve the corrosion resistance of the galvanized steel substrates. The morphological features of the coated substrates were evaluated before and after corrosion tests using atomic force microscopy (AFM) and scanning electron microscopy (SEM). The corrosion behavior of the sol–gel coatings was investigated using natural salt spray tests, electrochemical impedance spectroscopy (EIS), and potentiodynamic polarization tests. The results obtained in the present work show that the activation of the nanoparticles with cerium ions leads to the formation of thicker and more protective silane films.

## 2. EXPERIMENTAL

### 2.1. Sample preparation

Ceria nanoparticles (10 wt% in water, particle size < 25 nm, Sigma Aldrich) were ultrasonically dispersed in an aqueous solution of cerium nitrate (Fluka), to obtain concentrations of 0.025 M for the nanoparticles, and 0.025 M for the cerium nitrate. This aqueous dispersion was then used to prepare what will be called the “silane solution containing activated CeO<sub>2</sub> nanoparticles” in the remaining part of the paper.

Another set of ceria nanoparticles was ultrasonically dispersed in water at a concentration of 0.05 M. This aqueous dispersion was used to prepare what will be called the “silane solution containing CeO<sub>2</sub> nanoparticles” in the remaining part of the paper.

The silane solution was prepared by adding 4.084 mL of 3-glycidoxypropyltrimethoxy silane or GPTMS (Merck) to 0.5 mL of HCl-acidified water (pH = 2) (H<sub>2</sub>O/Si mole ratio = 0.5 [33]). The solution was placed in a sealed beaker and stirred at room temperature for 20 min at a rate of 240 rpm, to hydrolyze and condensate the silane precursors. The aqueous dispersion of ceria nanoparticles was added at the end of this synthesis step, and this was followed by stirring for 10 min. In the following step, 2.111 g of bisphenol A (BPA) (Merck) was added to the solutions as a cross-linking agent (BPA/Si mole ratio = 0.5). The latter has been shown to realize a significant effect on the morphology and improvement of the corrosion resistance of coatings [30]. The BPA was dissolved by mixing the solution for 80 minutes. To accelerate the condensation reaction, 0.0152 mL of 1-methylimidazol (MI) (Merck) (MI/Si mole ratio = 0.01) was added to the solution, which was followed by stirring for 5 min. The result was a clear and colorless homogenous solution.

Identical silane solutions were prepared with and without cerium nitrate, to obtain the so-called “cerium modified and non-modified silane coatings”. The Ce/Si mole ratio was 0.05.

The metallic substrate consisted of hot dip-galvanized steel coupons (4.98 cm<sup>2</sup> area and 0.1 cm thickness for the AFM, SEM, and electrochemical tests) and plates (7 × 15 × 0.1 cm for the salt spray tests). The zinc coating had a weight of approximately 140 g/m<sup>2</sup>, and a thickness of approximately 10 μm. The galvanized steel specimens were degreased using an alkaline cleaner. After cleaning, the substrates were washed with distilled water, dried in air, and immersed in the silane solution for 60 s. The coated specimens were dried at room temperature for 24 h, and subsequently submitted to a 25–130°C curing process for 90 minutes, to initiate extensive cross-linking in the hybrid films [34].

## 2.2. Analytical methods

Atomic force microscopy (AFM) images were obtained under ambient conditions using a Multimode scanning probe microscope (Digital Instruments – USA) equipped with a Nanoscope IIIa controller. Ten-micron scans were recorded in tapping mode, using a silicon cantilever (OTESPA – Veeco). Nanoscope software version 4.43r8 was used to analyze the surface roughness after the recorded images were modified using an X and Y Plane Fit Auto procedure.

Electrochemical impedance measurements (EIS) and potentiodynamic polarization tests were carried out to monitor the corrosion performance of the silane-treated galvanized steel substrates in a 3.5% NaCl solution, using an Autolab PG-STAT 20 potentiostat equipped with a frequency response analyzer module. A three-electrode system was used, in which an Ag/AgCl KCl<sub>sat</sub> electrode, a platinum mesh electrode, and the sample were used as reference, counter, and working electrodes, respectively. The EIS measurements were performed at the open circuit potential. The data were obtained as a function of frequency (frequency range of 10<sup>5</sup> Hz to 10<sup>-2</sup> Hz), using a sine wave with a peak-to-peak amplitude of 10 mV. All EIS measurements were carried out at room temperature, the samples were immersed in the electrolyte solution for 30 min before the data were acquired, and measurements were performed periodically. For each experiment, the measurements were repeated four times. Impedance fitting was performed using the appropriate equivalent circuits, in Z-view software (Scribner Associates Inc.).

The potentiodynamic measurements were performed within the range of -1500 to 1000 mV versus Ag/AgCl KCl<sub>sat</sub>, at a rate of 1 mV/s. These measurements were also performed four times. The Tafel extrapolation method (conducted according to the ASTM Standard G3-89, 2004) [36] was used to determine I<sub>corr</sub> and E<sub>corr</sub>.

Scanning electron microscopy (SEM) measurements were performed using an XL30 SEM microscope (FEI) equipped with energy dispersive X-ray spectroscopy. The aim was to characterize the microstructure, obtain qualitative chemical composition, and thickness of the coated substrates before and after the electrochemical impedance spectroscopy measurements (144 h of immersion in a 3.5% NaCl solution). Secondary electron images were collected at 20 kV.

The corrosion performance of the coated substrates was evaluated in a neutral salt spray test that followed the ASTM B117 procedure [35], using a 5% NaCl solution. Prior to exposure, the back and the edges of the plates were covered with adhesive tape. An artificial scratch that reached the substrate was made in the coating, to examine possible delamination. Visual assessment of the macroscopic surfaces was carried out at various time intervals throughout the total exposure time (144 h).

## 3. RESULTS AND DISCUSSION

### 3.1. Atomic force microscopy studies

Figure 1 presents AFM (a, c, e, g) top view and (b, d, f, h) topographic images taken of the HDG steel specimen coated with non-modified and cerium-modified silane coatings. The image in Figure 1a revealed a comparatively smooth nanostructured surface with a root mean square (RMS)

surface roughness of 0.608 nm. The image did not show much color contrast, which suggested low levels of heterogeneity in the coating thickness, and good distribution of the silica particles. However, the image in Figure 1b, which showed substrate features, revealed some large particles that likely resulted from the agglomeration of smaller particles on the surface [37-38]. These images were used as references to examine the changes in the surface morphology that occurred after the addition of the cerium dopant and the nanoparticles. In the case of the silane coating modified with  $\text{Ce}(\text{NO}_3)_3$ , the images (Figure 1c and d) revealed a smooth nanostructured surface with an RMS surface roughness of 0.402 nm. Interestingly enough, the rather low color contrast in Figure 1c suggested limited heterogeneity in the coating thickness. In addition, no agglomerates were present on the surface.

For the coating modified with  $\text{CeO}_2$  nanoparticles, the image (Figure 1e) revealed the presence of a number of  $\text{CeO}_2$  nanoparticles uniformly distributed in the silane coating, which had an RMS roughness of 8.421 nm. Some agglomerates were also visible on the topographic image (Figure 1f). Furthermore, there was a sharper color contrast in the topographic image, suggesting larger height differences. The color contrast was uniformly distributed throughout the image, which indicated the heterogeneity of the coating thickness; this was also observed by Phanasgaonkar et al. [38].

Figure 1g shows a top-view image of the silane film filled with activated  $\text{CeO}_2$  nanoparticles. The image revealed the presence of a number of  $\text{CeO}_2$  nanoparticles uniformly distributed in the silane coating, which had an RMS roughness of 6.210 nm. The figure did not show much color contrast, which indicated the lower heterogeneity of the coating thickness. In addition, the topographic image (1h) showed that the outer surface layers of this coating contained particles and agglomerates with nanometer-scale dimensions. These results suggest that addition of cerium ions altered the surface morphology of the coating modified with non-activated  $\text{CeO}_2$  nanoparticles.

### 3.2. Surface microstructure before and after electrochemical impedance spectroscopy tests

SEM analysis was used to investigate the effects of the  $\text{CeO}_2$  nanoparticles on the microstructure and qualitative chemical composition of the intact cerium-modified and non-modified silane coatings. Figure 2a shows the typical blank silane coating surface prior to immersion in a 3.5% NaCl solution. The coating appeared to be uniform, defect and crack-free. However, several white agglomerates appeared in the coating matrix, which were identified by EDX as being Si-rich (Figure 2b). It is likely that these features were clusters of nanoparticles formed in the outermost layers of the silane film [39-40]. The coatings doped with cerium nitrate and cerium oxide nanoparticles contained many particles of different sizes (Figure 2c and d, respectively). These particles were equally distributed in the coatings, and no micro-scale pores or cracks were observed. In the case of the silane film filled with  $\text{CeO}_2$  nanoparticles activated with cerium ions (Figure 2e), silica agglomeration was detected, but at lower levels, and with smaller particles compared to the blank silane film. EDX analysis of this region (Figure 2f) clearly showed the presence of cerium and silicon peaks. These results indicated that the addition of activated  $\text{CeO}_2$  nanoparticles led to the decomposition of the silane chains and a reduction in the size of the particles in the sols [38, 39].

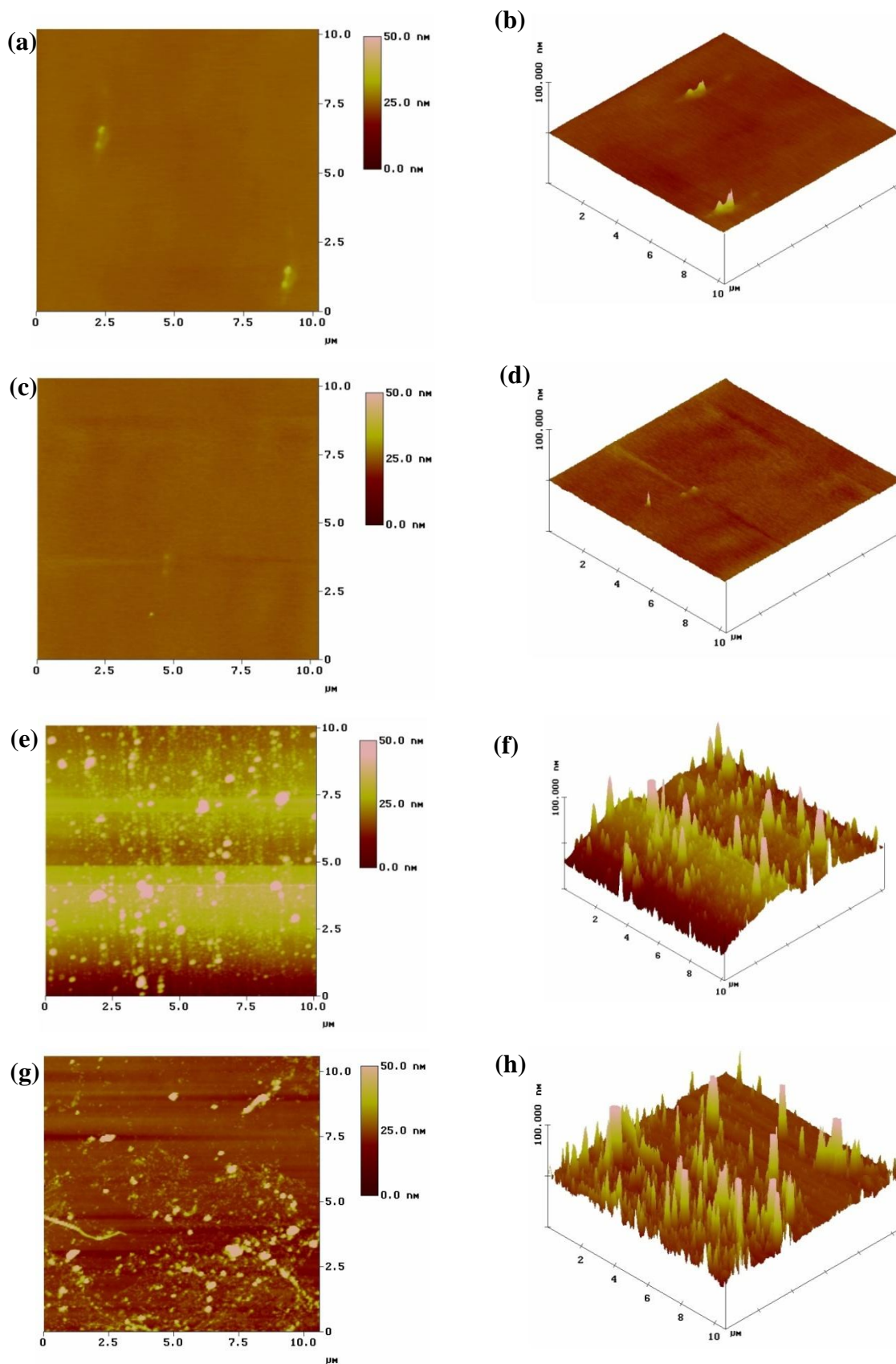


**Figure 1.** AFM top-view (a, c, e, g) and topographic images (b, d, f, h) of the HDG steel samples coated with blank silane (a, b), Ce(NO<sub>3</sub>)<sub>3</sub>·6H<sub>2</sub>O (c, d), CeO<sub>2</sub> nanoparticles (e, f), and CeO<sub>2</sub> + Ce(NO<sub>3</sub>)<sub>3</sub>·6H<sub>2</sub>O (g, h).

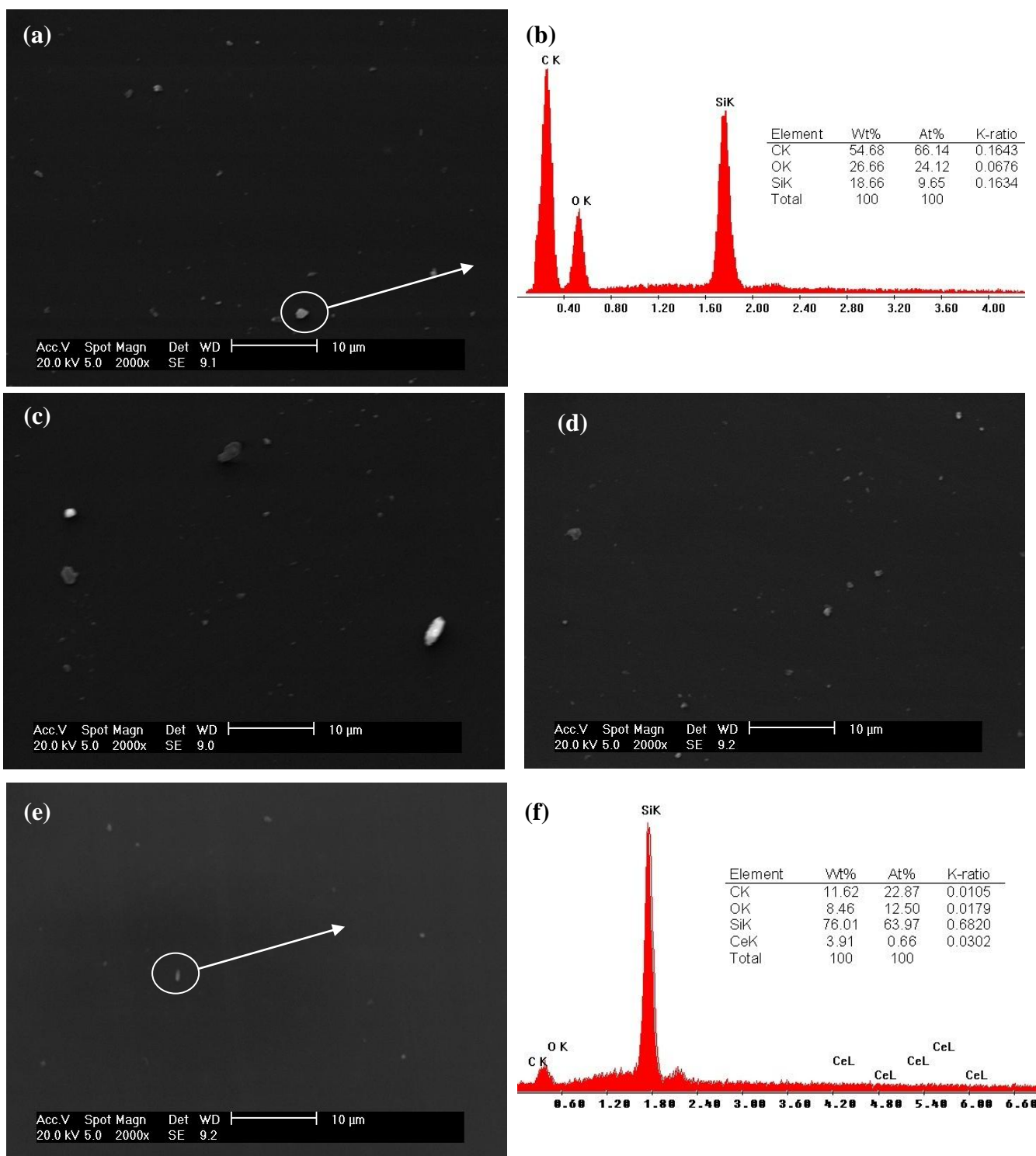


**Figure 2.** Scanning electron micrographs (a, c, d, e) and EDX spectrum obtained from the indicated regions (b, f) of the HDG steel samples coated with blank silane (a, b),  $\text{Ce}(\text{NO}_3)_3 \cdot 6\text{H}_2\text{O}$  (c),  $\text{CeO}_2$  nanoparticles (d), and  $\text{CeO}_2 + \text{Ce}(\text{NO}_3)_3 \cdot 6\text{H}_2\text{O}$  (e, f) prior to immersion in a 3.5% NaCl solution.

The thickness of the silane films was also determined using SEM. The silane coatings modified with cerium nitrate and cerium oxide nanoparticles showed thicknesses of approximately 2.16 and 4.97  $\mu\text{m}$ , respectively. These values increased to approximately 6.77  $\mu\text{m}$  for the films filled with  $\text{CeO}_2$  nanoparticles activated with cerium ions. All modified films were thicker than the blank silane film, which showed a thickness of approximately 1.89  $\mu\text{m}$ . These results suggested that a thicker or better cross-linked coating layer was formed in the presence of the activated cerium nanoparticles, as was also observed by Montemor et al. [19] and Garcia-Heras et al. [41]. This modification in the coating matrix can provide improved resistance to the oxidation of the substrate [38].

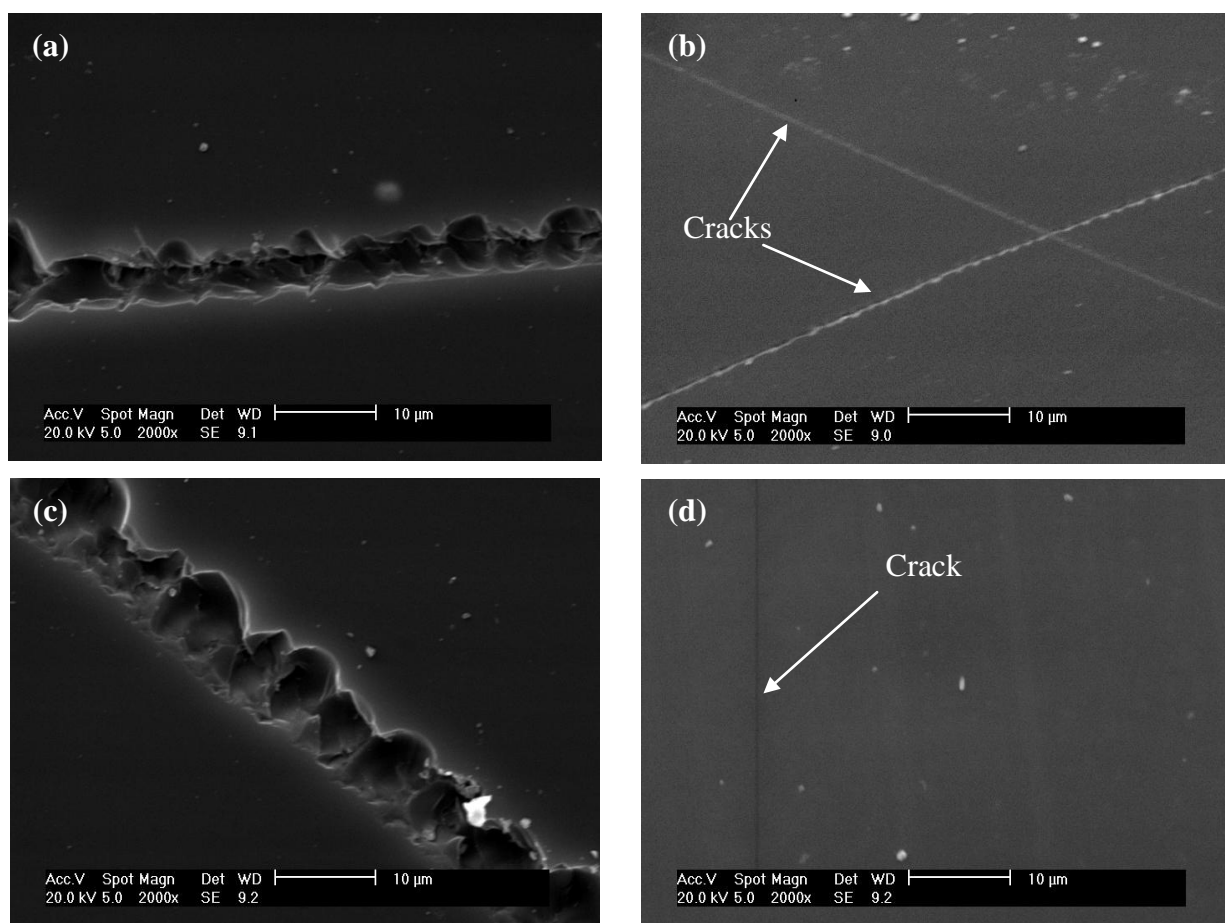


**Figure 3.** Scanning electron micrographs of the HDG steel samples coated with blank silane (a),  $\text{Ce}(\text{NO}_3)_3 \cdot 6\text{H}_2\text{O}$  (b),  $\text{CeO}_2$  nanoparticles (c), and  $\text{CeO}_2 + \text{Ce}(\text{NO}_3)_3 \cdot 6\text{H}_2\text{O}$  (d) after 144 h of immersion in a 3.5% NaCl solution.

The SEM images for the non-modified and cerium-modified silane coatings obtained after the electrochemical impedance spectroscopy tests are shown in Figure 3. The morphologies of the samples indicated the ability of the sol-gel coatings to protect the HDG steel substrates. After 144 h of immersion in a 3.5% NaCl solution, localized corrosion was observed for all coatings, which consisted of the exfoliation of the corrosion products and cracks of different sizes. These localized attacks promoted the deterioration and delamination of the hybrid film, possibly due to hydrolysis reactions at

the interface. Additionally, the diffusion of the oxidant ions became faster, and the corrosion rate increased, causing an accumulation of corrosion products at the interface, and at the same time promoting the formation of defects and micro-cracks [32]. However, the SEM results showed that the barrier properties of the films containing the activated nanoparticles (Figure 3d) were improved, likely as a consequence of the increased film thickness. The presence of the cerium ions also promoted the formation of reactive silanol groups in the silane molecules, leading to a higher degree of cross-linking, higher silicon content, and therefore more homogeneous films with better barrier properties, as has been confirmed by Montemor et al. [19].

### 3.3. Performance in salt spray tests

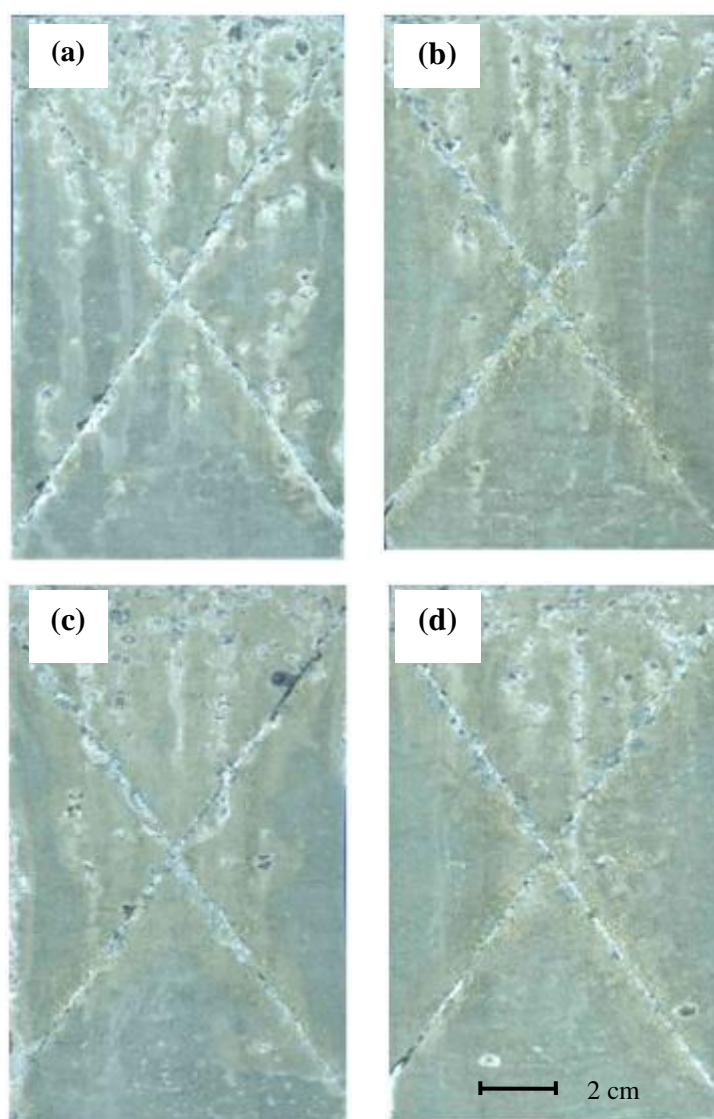


**Figure 4.** Photographs of the HDG steel samples coated with blank silane (a),  $\text{Ce}(\text{NO}_3)_3 \cdot 6\text{H}_2\text{O}$  (b),  $\text{CeO}_2$  nanoparticles (c), and  $\text{CeO}_2 + \text{Ce}(\text{NO}_3)_3 \cdot 6\text{H}_2\text{O}$  (d), after 144 h of salt spray exposure.

To detect possible differences among the differently modified silane films, salt spray testing was performed. Figure 4 presents the qualitative results of the exposure after 144 h. At the initial stages of exposure, all coatings showed the sacrificial dissolution of zinc in the artificially scratched area. As the salt spray analysis progressed, the breakdown of the coating layers progressed, and this was followed by the degradation of the zinc coatings, resulting in the formation of white rust [42].

For the blank silane-coated substrate, delamination increased rapidly with increasing salt spray exposure time. After modification of the silane coating, the delamination still increased with exposure time, but at markedly reduced rates. For example, for the silane coating filled with activated CeO<sub>2</sub> nanoparticles, comparatively little delamination was observed after exposure to the neutral salt spray for 144 h. This indicated the stable nature and barrier protection characteristics of the coating.

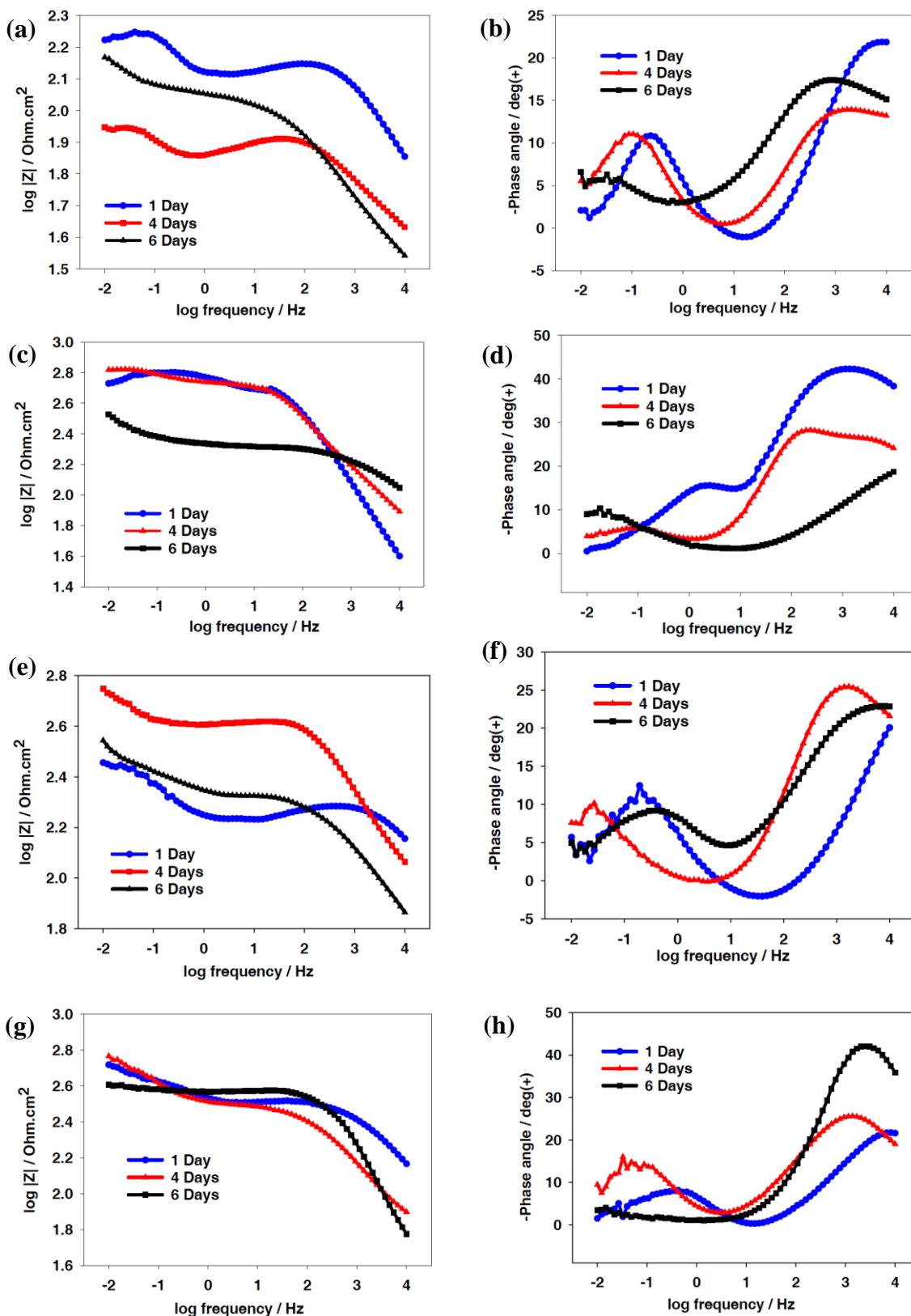
### 3.4. Electrochemical impedance spectroscopy

Figure 5a and c shows the electrochemical impedance spectra obtained on the galvanized steel substrates pre-treated with the non-modified and Ce(NO<sub>3</sub>)<sub>3</sub>-modified silane films, respectively. The results showed that the impedance values were higher for the film containing cerium nitrate. Furthermore, in the presence of cerium nitrate, the values for the total impedance remained approximately constant during the experiment (144 h in 3.5% NaCl solution). This effect was due to both the better barrier properties, and the corrosion inhibition abilities, as reported in a previous study [30].

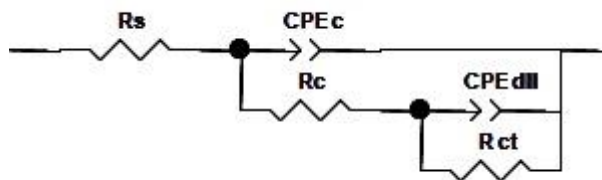
The EIS Bode plots obtained for the silane coatings filled with CeO<sub>2</sub> nanoparticles are shown in Figure 5e and g. The total impedance of the system was lower for the system containing only CeO<sub>2</sub>. The addition of cerium ions led to a significant increase in the impedance. For example, after 24 h of immersion, the total impedance of the CeO<sub>2</sub>-plus-cerium system was more than two orders of magnitude higher than that of the system filled with only CeO<sub>2</sub>. This trend was also noted in previous literature [9, 19], and was attributed to the fact that nanoparticles are likely to agglomerate and create large defects in the coating, promoting the uptake of the aggressive solution, and therefore promoting corrosion activity. The activation of the nanoparticles with cerium ions enhanced the protective properties of the modified silane films by increasing the film thickness and/or reducing the porosity [19].

The shape of the phase angle plot indicated the presence of two time constants (Figure 5b, d, f, h), which were attributed to the response of the silane film (high frequency process), and the response of the processes occurring at the silane film/substrate interface (low frequency time constant).

A more detailed interpretation of the EIS results can be made by numerical fitting, using the equivalent circuit depicted in Figure 6. In this equivalent circuit, constant phase elements were used instead of pure capacitors, because of the non-ideal character of the corresponding response with phase shifts differing from  $-90^\circ$ .

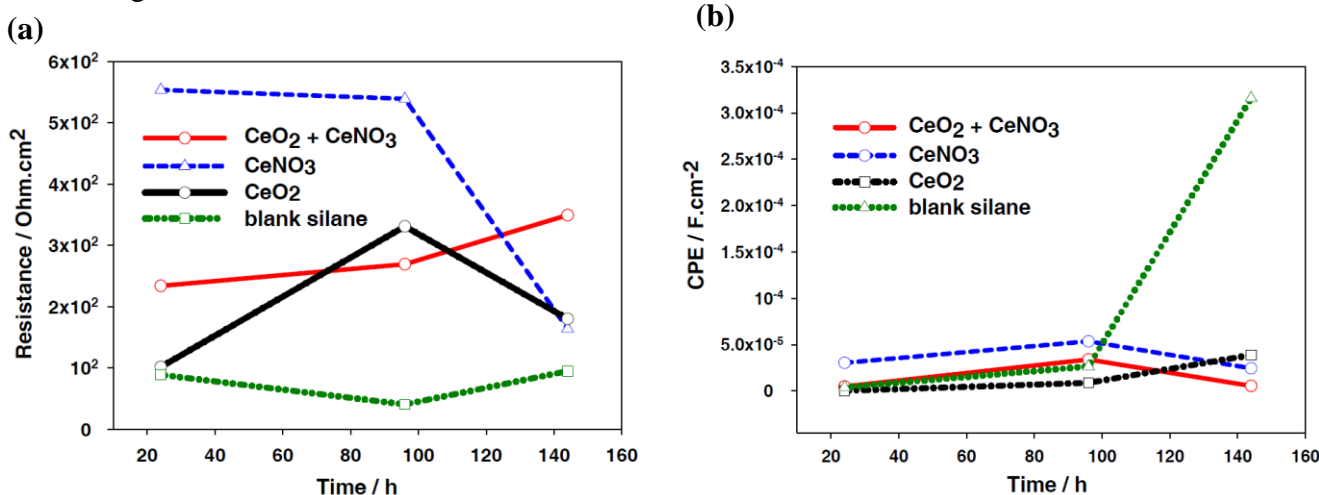


**Figure 5.** EIS Bode modulus (a, c, e, g) and phase angle (b, d, f, h) plots obtained on the HDG steel samples pre-treated with the blank silane coating (a, b), Ce(NO<sub>3</sub>)<sub>3</sub>.6H<sub>2</sub>O (c, d), CeO<sub>2</sub> nanoparticles (e, f), and CeO<sub>2</sub> + Ce(NO<sub>3</sub>)<sub>3</sub>.6H<sub>2</sub>O (g, h) during 144 h of immersion in a 3.5% NaCl solution.



**Figure 6.** Equivalent circuit used for the numerical fitting of the EIS data during immersion in a 3.5% NaCl solution.

The true capacitances were then calculated from the respective CPE parameters, as described elsewhere [30]. Thus, for the equivalent circuit shown in Figure 6,  $R_s$  is the resistance of the electrolyte;  $CPE_C$  and  $R_C$  represent the capacitance and resistance of the hybrid coating, respectively;  $CPE_{dl}$  is the capacitance of the electrochemical double layer at the metal/electrolyte interface; and  $R_{ct}$  is the charge transfer resistance of the metal.



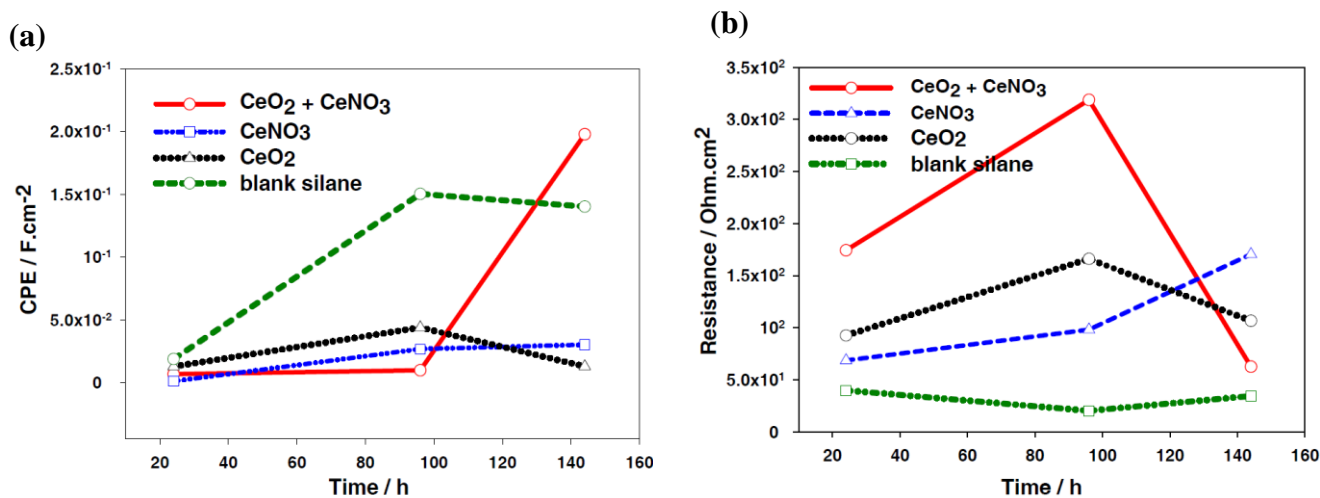
**Figure 7.** Evolution of the coating resistance (a), and coating capacitance (b), during immersion in a 3.5% NaCl solution. Values were obtained by numerical fitting, using the equivalent circuit depicted in Figure 6.

Figure 7 shows the evolution of the coating properties (i.e. the resistance and capacitance) as a function of immersion time. Generally, the high-frequency resistance values (Figure 7a) showed a decrease during the first hours of immersion, due to the development of conductive pathways inside the blank silane film [8]. After the start of immersion, the highest resistance was observed for the coating modified with Ce(NO<sub>3</sub>)<sub>3</sub>; this was followed by a sharp drop after a few hours. For the coating with non-activated CeO<sub>2</sub> nanoparticles, the high frequency resistance passed through a maximum, and then started to decrease. The initial increase of the high-frequency resistance values in the last two systems was attributed to swelling of the matrix and the consequent closing of nano/micro pores [43].

The evolution of the high-frequency resistance for the system filled with activated  $\text{CeO}_2$  nanoparticles showed a more gradual increase. During the first hours of immersion, the EIS response was nearly capacitive over the entire frequency range, and the resistance values were above  $233 \Omega \text{ cm}^2$ . The resistance slowly increased during the experiment and after 144 h (6 days) the resistance showed a significant increase. Compared with the blank silane film, the modified silane films showed significantly improved barrier properties.

The evolution of the coating capacitance is shown in Figure 7b. The silane coating filled with activated  $\text{CeO}_2$  nanoparticles had the lowest capacitance of the four systems examined over the 144 h of immersion, and had the largest coating thickness. Further, the capacitance showed relatively consistent values during immersion, with only a small increase after 96 h of immersion; this was associated with uptake of the electrolyte [9, 43]. In contrast, after 96 h of immersion, a significant increase in film capacitance was observed for the sample pretreated with the blank silane film, as a result of the water uptake that occurred due to the reduced barrier properties of the film [9].

The evolution of the high frequency fitting parameters indicated that the addition of nanoparticles reinforced the barrier properties of the film. The addition of cerium to the nanoparticles markedly influenced the capacitance and resistance of the coatings, and then systems filled with cerium-activated  $\text{CeO}_2$  nanoparticles were more protective than the other systems. These results were in accordance with Schem et al.'s work on aluminum alloys with a silane coating filled with  $\text{CeO}_2$  nanoparticles [43], and Montemor et al.'s work on galvanized steel with silane coatings doped with Ce salt-activated nanoparticles [9].



**Figure 8.** Evolution of the double layer capacitance (a) and the transfer resistance (b) during immersion in a 3.5% NaCl solution. Values were obtained by numerical fitting using the equivalent circuit depicted in Figure 6.

The evolution of the fitting parameters associated with the low frequency behavior of the EIS spectra (Figure 8) gave information on the electrochemical activity at the silane/zinc interface. For the

system pre-treated with the silane coating, the initial CPE values (Figure 8a) were of the order of  $0.0187 \text{ F cm}^{-2}$ . During 96 h of immersion, the CPE values increased and then stabilized at approximately  $0.1402 \text{ F cm}^{-2}$ . This agreed with the evolution of the low frequency resistance (Figure 8b) of the blank silane films, which showed a gradual decrease during the 96 h of immersion, from  $39.81 \text{ } \Omega \text{ cm}^2$  to  $20.24 \text{ } \Omega \text{ cm}^2$ ; the resistance then stabilized at approximately  $34.42 \text{ } \Omega \text{ cm}^2$ .

Distinctive behavior was observed in the systems modified with  $\text{CeO}_2$ . In the absence of cerium ions, after 96 h of immersion, the  $\text{CeO}_2$ -filled system showed CPE values of approximately  $0.0438 \text{ F cm}^{-2}$ , and resistances that increased from  $92.54 \text{ } \Omega \text{ cm}^2$  (during the first hour of immersion) to approximately  $166.20 \text{ } \Omega \text{ cm}^2$ . After 144 h of immersion, the CPE and the resistance had increased by small amounts to  $0.0129 \text{ F cm}^{-2}$  and  $106.60 \text{ } \Omega \text{ cm}^2$ , respectively. The activation with cerium ions had significant effects on both the low frequency CPE and the resistance. During the 96 h of immersion, the CPE values were below  $9.7601 \times 10^{-3} \text{ F cm}^{-2}$ , and the resistances increased to over  $318.80 \text{ } \Omega \text{ cm}^2$ . As the immersion time elapsed, there was a gradual decrease in resistance. Finally, the resistance and CPE values approached the values observed for the silane coating modified with  $\text{Ce}(\text{NO}_3)_3$ . The low frequency resistance increased with immersion time, indicating that the cerium oxide/hydroxide was stably formed with the release of  $\text{Ce}(\text{NO}_3)_3$  from the sol-gel matrix [44]. The low frequency resistance value slowly increased to close to  $170.62 \text{ } \Omega \text{ cm}^2$  after 144 h of immersion, indicating the continuous accumulation of the cerium oxide/hydroxide over the immersion period. In addition, the CPE value increased gradually to approximately  $0.0301 \text{ F cm}^{-2}$  after 144 h of immersion, four orders of magnitude lower than the value measured for the blank silane coating, suggesting that the inhibition products had filled the originally electrolyte-saturated pores at the coating/substrate interface [44].

In some cases, the evolution of the low frequency resistance showed an increase after a few hours, accompanied by a decrease in the CPE. Since the corrosion activity occurred in localized areas, it is likely that the precipitation of the insoluble and passive corrosion products occurred at these locations, decreasing the corrosion activity at the interface [9]. In fact, the most pronounced changes were observed for the blank silane film, which was the one that presented the poorest barrier properties and was therefore the most prone to early corrosion attack, as was observed by Montemor et al. [9].

### 3.5. Potentiodynamic polarization results

The polarization curves of the specimens, which were recorded after 1 h of immersion in the electrolyte, are illustrated in Figure 9. The corrosion current ( $i_{\text{corr}}$ ) and corrosion potential ( $E_{\text{corr}}$ ) were determined using Tafel extrapolation [36, 39]. The relevant parameters (Table 1) indicate the different effects of the cerium modification on the  $i_{\text{corr}}$  and  $E_{\text{corr}}$  of the silane coatings. There were two notable differences in the curve's features for the samples pre-treated with the blank silane film and the samples treated with the silane film filled with activated  $\text{CeO}_2$  nanoparticles. One of the differences was the large shift in the  $E_{\text{corr}}$  value to a less negative value, and the other was related to the marked reduction in the cathodic current density ( $\text{A/cm}^2$ ). The difference in  $E_{\text{corr}}$  directly reflected the degree of coverage of the coating over the entire substrate [45]. The good coverage provided a continuous nanoporous coating layer, and caused the shift of the  $E_{\text{corr}}$  value to a more positive value. The difference in the cathodic current density was attributed to the inhibiting aspects of the cathodic

reaction at the corrosion site, particularly the oxygen reduction reaction [45, 46]. Similar behavior has been reported by Montemor et al. [9] for galvanized steel substrates in a 0.005 M NaCl solution.

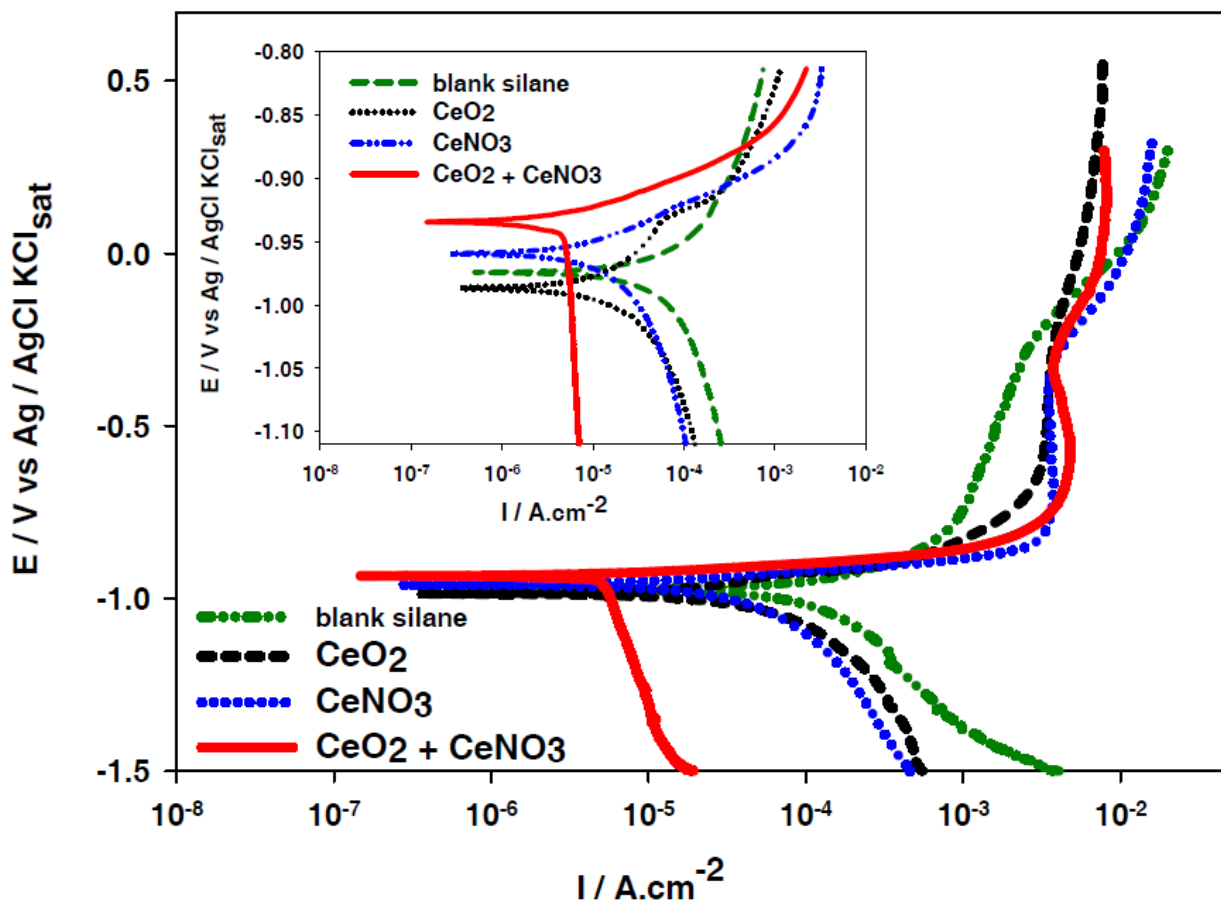


**Figure 9.** Potentiodynamic polarization curves for the HDG steel samples coated with blank silane,  $\text{Ce}(\text{NO}_3)_3 \cdot 6\text{H}_2\text{O}$ ,  $\text{CeO}_2$  nanoparticles, and  $\text{CeO}_2 + \text{Ce}(\text{NO}_3)_3 \cdot 6\text{H}_2\text{O}$ , obtained after 1 h of immersion in a 3.5% NaCl solution. For comparative purposes, the inset shows a plot in which the potential is depicted as the difference between the imposed potential and the corrosion potential. This approach allows a better separation of the anodic and cathodic polarization effects.

**Table 1.** Summary of the electrochemical parameters obtained from the polarization, measured in a 3.5% NaCl solution.

| Sample                                    | $E_{\text{corr}}$ (V) | $I_{\text{corr}}$ ( $\text{A cm}^{-2}$ ) | $b_c$ (V/dec) | $b_a$ (V/dec) | Passive area (V) |
|---|-----------------------|--|---------------|---------------|------------------|
| Blank silane                              | -0.974                | $3.577 \times 10^{-5}$                   | 0.06          | 0.093         | -0.792 to -0.241 |
| $\text{Ce}(\text{NO}_3)_3$                | -0.959                | $3.224 \times 10^{-6}$                   | 0.022         | 0.022         | -0.832 to -0.320 |
| $\text{CeO}_2$                            | -0.987                | $4.904 \times 10^{-6}$                   | 0.031         | 0.026         | -0.677 to -0.262 |
| $\text{CeO}_2 + \text{Ce}(\text{NO}_3)_3$ | -0.934                | $1.116 \times 10^{-6}$                   | 0.015         | 0.012         | -0.809 to -0.327 |

#### 4. CONCLUSIONS

Pre-treatments of hot dip-galvanized steel based on the use of 3-glycidoxypropyltrimethoxysilane (GPTMS) and bisphenol A (BPA) filled with activated CeO<sub>2</sub> nanoparticles revealed the formation of a comparatively smooth nanostructured surface, with low heterogeneity in the coating thickness. Microscopic observations also confirmed that the complete surface morphology of the silane coating filled with activated CeO<sub>2</sub> nanoparticles was maintained after short-term corrosion tests (144 h immersion in 3.5% NaCl solution). These coatings resisted the salt spray exposure for 144 h, with reduced corrosion near an artificial scratch, and uniform corrosion otherwise, which contrasted with the blank silane coating.

Upon the addition of activated CeO<sub>2</sub> nanoparticles as a dopant, the silane coating showed improved barrier properties and coating resistance, and a decrease in coating capacitance. The incorporation of activated CeO<sub>2</sub> nanoparticles reduced the cathodic current density by two orders of magnitude, and shifted the voltage to more positive values (compared with the blank silane-coated substrate) during polarization in a 3.5% NaCl solution.

#### ACKNOWLEDGEMENTS

The authors wish to acknowledge Ghent University for financial support of this study and Arcelor Mittal Gent for providing the material. The authors would also like to thank Michel Moors, Christa Sonck, and Sandra Van Vlierberghe for technical assistance.

#### References

1. I.A. Kartsonakis, A.C. Balaskas, E.P. Koumoulos, C.A. Charitidis, G.C. Kordas, *Corros. Sci.*, 57 (2012) 30.
2. A.R. Marder, *Prog. Mater. Sci.*, 45 (2000) 191.
3. A.M.P. Simoes, R.O. Carbonari, A.R. Di Sarli, B. Del Amo, R. Romagnoli, *Corros. Sci.*, 53 (2011) 464.
4. J.B. Bajat, V.B. Miskovic-Stankovic, J.P. Popic, D.M. Drazic, *Prog. Org. Coat.*, 63 (2008) 201.
5. M. Taryba, S.V. Lamaka, D. Snihirova, M.G.S. Ferreira, M.F. Montemor, W.K. Wijting, S. Towes, G. Grundmeier, *Electrochim. Acta*, 56 (2011) 4475.
6. B. Ramezanzadeh, M.M. Attar, *Prog. Org. Coat.*, 71 (2011) 314.
7. B. Ramezanzadeh, M.M. Attar, *Surf. Coat. Technol.*, 205 (2011) 4649.
8. M.F. Montemor, R. Pinto, M.G.S. Ferreira, *Electrochim. Acta*, 54 (2009) 5179.
9. M.F. Montemor, M.G.S. Ferreira, *Electrochim. Acta*, 52 (2007) 6976.
10. M.L. Zheludkevich, R. Serra, M.F. Montemor, K.A. Yasakau, I.M. Miranda Salvado, M.G.S. Ferreira, *Electrochim. Acta*, 51 (2005) 208.
11. M.L. Zheludkevich, M.F. Montemor, I.M. Salvado, M.G.S. Ferreira, *Electrochem. Commun.*, 7 (2005) 836.
12. Y. Castro, B. Ferrari, R. Moreno, A. Duran, *Surf. Coat. Technol.*, 182 (2004) 199.
13. M.F. Montemor, A.M. Cabral, M.L. Zheludkevich, M.G.S. Ferreira, *Surf. Coat. Technol.*, 200 (2006) 2875.
14. V. Palanivel, D. Zhu, W.J. van Ooij, *Prog. Org. Coat.*, 47 (2003) 384.
15. L. Liu, J.-M. Hu, J.-Q. Zhang, C.-N. Cao, *Electrochim. Acta*, 52 (2006) 538.
16. M.F. Montemor, M.G.S. Ferreira, *Prog. Org. Coat.*, 60 (2007) 228.

17. A. Franquet, H. Terryn, J. Vereecken, *Thin Solid Films*, 441 (2003) 76.
18. T. Van Schaftingen, C. Le Pen, H. Terryn, F. Hörzenberger, *Electrochim. Acta*, 49 (2004) 2997.
19. M.F. Montemora, M.G.S. Ferreira, *Prog. Org. Coat.*, 63 (2008) 330.
20. M. Aresta, A. Dibenedetto, C. Pastore, C. Cuocci, B. Aresta, S. Cometa, E. De Giglio, *Catal. Today*, 137 (2008) 125.
21. M. Dudek, *J. Eur. Ceram. Soc.*, 28 (2008) 965.
22. A. Trinchi, Y.X. Li, W. Wlodarski, S. Kaciulis, L. Pandolfi, S. Viticoli, E. Comini, G. Sberveglieri, *Sens. Actuators B: Chem.*, 95 (2003) 145.
23. N. Izu, T. Itoh, W. Shin, I. Matsubara, N. Murayama, *Sens. Actuators B: Chem.*, 123 (2007) 407.
24. Y. Yang, J.L. Ong, J. Tian, *Biomaterials*, 24 (2003) 619.
25. S.M.A. Shibli, F. Chacko, *Surf. Coat. Technol.*, 202 (2008) 4971.
26. S. Zhang, M. Li, J.H. Yoon, T.Y. Cho, C.G. Lee, Y. He, *Appl. Surf. Sci.*, 254 (2008) 7446.
27. Y. Wang, Z. Wang, Y. Yang, W. Chen, *Intermetallics*, 16 (2008) 682.
28. D. Nickolova, E. Stoyanova, D. Stoychev, I. Avramova, P. Stefanov, *Surf. Coat. Technol.*, 202 (2008) 1876.
29. R. Xu, J. Wang, L. He, Z. Guo, *Surf. Coat. Technol.*, 202 (2008) 1574.
30. R. Zandi Zand, K. Verbeken, A. Adriaens, *Prog. Org. Coat.*, 75 (2012) 463.
31. R. Zandi Zand, K. Verbeken, A. Adriaens, *Int. J. Electrochem. Sci.*, 7 (2012) 9592.
32. R. Zandi Zand, K. Verbeken, A. Adriaens, *Int. J. Electrochem. Sci.*, 8 (2013) 548.
33. R.Z. Zand, Investigation of corrosion, abrasion and weathering resistance in hybrid nanocomposite coatings based on epoxy-silica, Thesis, Azad University-Tehran North Branch, (2005).
34. R. Zandi Zand, K. Verbeken, A. Adriaens, *Prog. Org. Coat.*, 72 (2011) 709.
35. ASTM B117 - 11 Standard Practice for Operating Salt Spray (Fog) Apparatus, G01.05, Book of Standards Volume: 03.02 (2011).
36. ASTM Standards for Corrosion Testing of Metals: 3rd Edition, ASTM International, W. Conshohocken, PA, (2008).
37. M.F. Montemor, W. Trabelsi, S.V. Lamaka, K.A. Yasakau, M.L. Zheludkevich, A.C. Bastos, M.G.S. Ferreira, *Electrochim. Acta*, 53 (2008) 5913.
38. A. Phanasgaonkar, V.S. Raja, *Surf. Coat. Technol.*, 203 (2009) 2260.
39. X. Zhong, Q. Li, J. Hu, X. Yang, F. Luo, Y. Dai, *Prog. Org. Coat.*, 69 (2010) 52.
40. Luis M. Palomino, Patricia H. Suegama, Idalina V. Aoki, M.F. Montemor, Hercílio G. De Melo, *Corros. Sci.*, 51 (2009) 1238.
41. M. Garcia-Heras, A. Jimenez-Morales, B. Casal, J.C. Galvan, S. Radzki, M.A. Villegas, *J. Alloys Comp.*, 380 (2004) 219.
42. S.M.A. Shibli, Francis Chacko, *Surf. Coat. Technol.*, 205 (2011) 2931.
43. M. Schem, T. Schmidt, J. Gerwann, M. Wittmar, M. Veith, G.E. Thompson, I.S. Molchan, T. Hashimoto, P. Skeldon, A.R. Phani, S. Santucci, M.L. Zheludkevich, *Corros. Sci.*, 51 (2009) 2304.
44. H. Shi, F. Liu, E. Han, *Mater. Chem. Phys.*, 124 (2010) 291.
45. T. Sugama, *JCT Res.*, 2 (2005) 649.
46. M. Hosseini, H. Ashassi-Sorkhabi, H. Yaghobkhani Ghiasvand, *J. Rare. Earth*, 25 (2007) 537.